

# THREE-DIMENSIONAL SIMULATIONS OF GASTRIC BIOMAGNETIC DIPOLES USING RECURSIVE LOCALIZATION ALGORITHMS

Andrei Irimia

Living State Physics Laboratories  
Department of Physics and Astronomy  
Vanderbilt University  
6301 Stevenson Science Center  
Nashville, Tennessee, 37235, USA

Biomagnetism Laboratory  
Department of Physics and Astronomy  
Vanderbilt University  
6301 Stevenson Science Center  
Nashville, Tennessee, 37235, USA

Department of Computing  
and Information Systems  
Lipscomb University  
3901 Granny White Pike  
Nashville, Tennessee, 37204, USA

## Abstract

The reconstruction of the stomach's biomagnetic field is a challenging visualization task with significant applications to the diagnosis of stomach disorders. The results of a new computation-based approach to the inverse problem are presented here in addition to how they apply to the reconstruction of the stomach's magnetic field. One of the primary advantages of the procedure is a realistic view of the magnetic field based on known experimental data using an efficient algorithm whose running time increases linearly as data input amounts increase. The program was tested using experimental data collected using SQUID magnetometers while the visual reconstruction of the biomagnetic field was accomplished in MATLAB using streamline vector field plots and color-based mappings of magnetic field data obtained using standard methods in electromagnetic field theory. In order to ensure exactness and reliability, results were compared to similar ones that had been obtained using purely theoretical reconstruction techniques. The visualization tool that has been developed is important for furthering our understanding of how anomalies in the gastric electromagnetic field can predict various pathological conditions.

**Key Words:** Biomagnetic Simulation, Inverse Problem, Signal Processing.

## 1. Introduction

A great deal of research has been dedicated to the subject of noninvasive biomagnetic research and how it is useful for studying various pathological manifestations that are important in medical diagnostics. In spite of considerable technical advances witnessed by this field in recent years, a great deal of complex and unanswered questions remain due to the inherent difficulty of studying biophysical systems. This situation often translates into a high level of difficulty in formulating mathematical models of these systems. Even in the case of scientific topics of great interest, such as the inverse biomagnetic problem, there is much to be learned about the processes that govern living organisms as a whole.

## 2. Theoretical Considerations

The inverse biomagnetic problem is of great importance to the study of human organs as well as to the diagnosis of a number of diseases. In the stomach, Gastric Electrical Activity (GEA) originates in the corpus and propagates toward the pylorus at a frequency of approximately 3 cycles per minute in humans and 7-8 cycles per minute in rabbits. It has been verified that changes in the propagation of the electrical activity caused by pathological states are measurable non-invasively and very useful in numerous clinical applications. Pathological states can be identified through the aid of the magnetogram (MGG) and magnetoenterogram (MENG), which record magnetic fields associated with the electrical activity of the stomach and small bowel. Given a region in the stomach exhibiting electric current flow and for which the distribution of current sources is known, the forward biomagnetic problem consists of solving Laplace's equation and then using Ohm's law to obtain the values for the electric potential  $V$  and current density  $J$ . The Biot-Savart law can be used to obtain the value of the magnetic field  $B$  using knowledge of the former two. The inverse process is naturally called the inverse problem and it consists of determining the sources of electric current given a set of experimentally recorded values of the magnetic field. The first step involved in the typical mathematical process of computing the value of  $B$  consists of analyzing the geometrical configuration of the region through which the electric current flows. Obtaining realistic solutions for this inverse problem is unfortunately not straightforward in most situations. In particular, its three-dimensional expression, which is also discussed here, does not have a unique solution due to the nature of Laplace's equation.

Solving the inverse problem for gastrointestinal sources of magnetic current is of great importance for the diagnosis of pathological conditions. Numerous techniques have been developed for finding realistic, anatomically relevant solutions [1]; as some specialists have pointed out, however, the general disadvantage of many analytical methods is that the characteristics of the biomagnetic dipoles and fields obtained often provide little insight into the biomedical mechanisms at work

within the system being studied [2]. One of the methods that have been developed consists of determining the location and orientation of the current dipole generating the magnetic field based on a least squares approximation approach. This article presents the theoretical background of a modified alternative to this computational approach and shows how solutions to the inverse problem apply to the reconstruction of the gastric magnetic field using a three-dimensional simulation program. One important advantage of the method below is that it offers a realistic visualization of the field based on known experimental data in linear computation time.

In one of the most common models of gastric biomagnetic behavior, the assumption is made that the current density in the stomach is well behaved and positioned in a finite region such that an enclosing surface can be formed outside this region. In order to obtain an expression of the magnetic field, it is sufficient to solely observe the radial component of the magnetic field. A particularly useful form of the Biot-Savart law can then be employed to reconstruct the magnetic field within the stomach [3]:

$$B_z = \frac{\mu_0}{4\pi} \iiint_G \mathbf{J}^i(\mathbf{r}) \times \frac{(\mathbf{r} - \mathbf{r}_0)}{|\mathbf{r} - \mathbf{r}_0|^3} d^3\mathbf{r} \quad (1)$$

where  $\mathbf{J}^i$  is the impressed current density in the stomach,  $B_z$  is the component of the biomagnetic field in the direction of the  $\mathbf{k}$  unit vector, and the constant  $\mu_0$  stands for the permeability of free space. The vector  $\mathbf{r}$  extends from the origin of the coordinate system to the measurement point of the magnetic field vector component  $B_z$ . Analogously,  $\mathbf{r}_0$  is the vector from the origin of the coordinate system to the position of the current dipole. Triple antidifferentiation is performed over a small volume  $G$  with  $\mathbf{r}_0$  in  $G$ . Since a current dipole with a moment  $\mathbf{Q}$  can be considered as a concentration of the impressed current to a single point, two important expressions can be derived:

$$\phi = \iiint_G \mathbf{J}^i(\mathbf{r}) d^3\mathbf{r} \quad (2)$$

$$\mathbf{J}(\mathbf{r}_0) = \iiint_G \phi \delta(\mathbf{r} - \mathbf{r}_0) d^3\mathbf{r} \quad (3)$$

where  $\delta$  is the Dirac delta function. Making use of the formulas above and performing the appropriate substitutions eventually leads to the expression

$$\mathbf{B} = \frac{\mu_0}{4\pi} \iiint_G \mathbf{J}^i(\mathbf{r}_0) \times \frac{(\mathbf{r} - \mathbf{r}_0)}{|\mathbf{r} - \mathbf{r}_0|^3} d^3\mathbf{r} \approx \frac{\mu_0}{4\pi} \frac{\mathbf{Q} \times (\mathbf{r} - \mathbf{r}_0)}{|\mathbf{r} - \mathbf{r}_0|^3} \quad (4)$$

The equation above can be very useful for performing a computation whose end result is obtaining a reconstruction of  $\mathbf{B}$  within a three-dimensional volume in which the stomach is located [4]. For example,

$$B_x = \frac{\mu_0}{4\pi} \frac{1}{|\mathbf{r} - \mathbf{r}_0|^3} [Q_y(z - z_0) - Q_z(y - y_0)] \quad (5)$$

and the other similar vector component forms of  $\mathbf{Q}$  in this formula above can easily be used to perform the reconstruction of the magnetic field.

### 3. Experiment Description

In the case of the application described in the remaining part of this article, biomagnetic fields were reconstructed from input data collected using a Superconducting QUantum Interference Device (SQUID) magnetometer. Subjects were placed horizontally under the sampler while the apparatus was configured so that its superconducting pick-up coils were allowed to record the individual vector values of the magnetic field passing through the stomach. The collected data were simultaneously stored in binary file format for further processing. A visual exemplification of the experimental arrangement is shown in Figure 1. A number of 29 SQUID channels (measurement coils) were used for magnetic field input, each of which was programmed with the ability to record values for one of the three magnetic field vector components. Five channels recorded the values of  $B_x$ , five those of  $B_y$ , and the remaining 19 recorded the values of  $B_z$ . Channels whose input was the  $\mathbf{z}$  component of  $\mathbf{B}$  were distributed in a formation resembling the shape of a hexagon. From the computational perspective of this arrangement, the vector  $(\mathbf{r} - \mathbf{r}_0)$  extends for each of the input channels from the position of the current dipole to the measurement point of the magnetic field  $\mathbf{B}$  (the pick-up coil of each channel). For each of the 29 input channels, the corresponding experimental values of the magnetic field, denoted by  $\tilde{B}_z$ , were converted from analog to digital format and stored in a binary file at a sampling frequency of 200 Hz. Experimental values were contained in a matrix  $\mathbf{M}$  of size  $b \times c$  where columns correspond to the  $c$  SQUID input channels while each row contains the experimental data recorded at every measurement moment numbered 1, 2, ...,  $b$ .

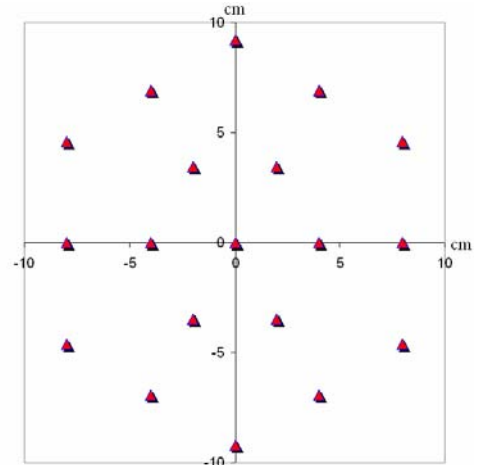


Figure 1. SQUID channels recording biomagnetic activity are located in concentric hexagonal formation above the stomach. The subject is

positioned with the head toward the top of the figure, facing up. The origin of the coordinate system is located at the center of the abdomen.

#### 4. Computational Approach

In order to construct a three-dimensional visualization of the magnetic field in the stomach, a sufficiently dense rectangular grid of  $29 \times 29$  points was created with its centroid positioned at location  $(0, 0, 0)$ , as in Figure 1. This ensured that a rearrangement of channel positions would not affect the configuration of the computational rectangle of interest. This flexibility was made available by allowing the input points to be positioned at any set of coordinates above the subject's stomach, which provides a straightforward manner of modifying the configuration of the channels without losing the full capabilities of the simulation. The dimensions of the grid were also determined so that its extremities coincided with the coordinate positions of the outermost channels. Finally, a reconstruction matrix that can be visualized as a three-dimensional tetrahedron was created and positioned with half of its volume above the level of the abdomen (taken to be  $z=0$ ) and half below it. A visual representation of this setup can be seen in Figure 2. For each sequential time recording of data in the matrix  $M$ , the magnetic field was reconstructed in the planar grid as well as in the three-dimensional tetrahedron. Due to the fact that input data was not available for all grid nodes, the methods of cubic interpolation and Delaunay triangulation were used in order to modify the data set into the format required for plotting the magnetic field at coordinates inside the hexagon-like channel structure. In addition, data was interpolated using a standard numerical method of calculating derivatives based on a forward-difference algorithm. Specifically, this was done for the set of grid components outside the SQUID magnetometer input area. For every case discussed below, the vector components of the current dipole were found according to the principles of least-squares approximation in which the squared errors in the computed values of the field components were minimized, i.e.,

$$\frac{\partial}{\partial Q_x} \left[ \sum_{j=1}^n \sum_{k=1}^m (\tilde{B}_z^{jk} - \hat{B}_z^{jk})^2 \right] = 0 \quad (8)$$

$$\frac{\partial}{\partial Q_y} \left[ \sum_{j=1}^n \sum_{k=1}^m (\tilde{B}_z^{jk} - \hat{B}_z^{jk})^2 \right] = 0 \quad (9)$$

where  $\tilde{B}_z$  stands for the experimental value of  $B_z$  (the value recorded by the SQUID magnetometer) while  $\hat{B}_z$  stands for its computed (reconstructed) value. The double summation from 1 to  $n$  and from 1 to  $m$  indicates that values were computed over the entire  $n \times m$  grid. Naturally, in the particular case of the example described here,  $n$  and  $m$  are both equal to 29. The superscripts  $j$  and  $k$  for the magnetic field component values indicate the subscripts in the grid of each magnetic field value. Magnetic field values were computed in the three-dimensional space of the stomach at a set of chosen

locations on the grid according to the forward biomagnetic model. These locations corresponded to the centroids of eight regions with equal areas into which the original grid region was divided. For each of these eight locations within the eight regions, values were computed for the total goodness of fit function  $\chi^2$ :

$$(\chi^2)_i = \sum_{j=1}^n \sum_{k=1}^m \frac{(\tilde{B}_z^{jk} - \hat{B}_z^{jk})^2}{(\delta_z^{jk})^2} \quad (10)$$

where the subscript  $i$  stands for the  $i$ -th of the eight regions within which values for  $\mathbf{B}$  were computed and  $\delta_z$  represents the error in the measurement of the  $B_z$  at the location indicated by the grid node superscripts  $j$  and  $k$ . Based on the values of the function  $\chi^2$  computed as described above, one sector of the grid was chosen where its function value was minimum among those for the eight sectors. Using a recursive algorithm, the chosen grid sector was subsequently divided into another set of sub-sectors. For each of these, the procedure described above was repeated in that the value of the average goodness of fit function was computed after performing the calculations for minimizing forward model magnetic field errors as in (8) and (9). The process was continued until the best fitting location for the position of the dipole was found on the measurement grid. This situation corresponds to the degenerate case of the recursion process in which the problem of finding better approximations of the dipole location can no longer be broken down into smaller identical problems due to the finite number of points in the grid.

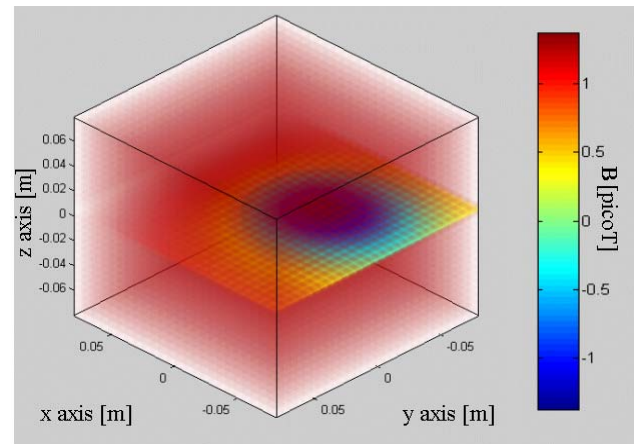


Figure 2. Visual depiction of the biomagnetic reconstruction arrangement used for the simulation. Experimental data is recorded non-invasively at the surface of the abdomen in a plane with equation  $z = 0$ , for which biomagnetic data is shown above in the form of a rectangular grid. The volume of the tetrahedron in which the grid is contained represents the portion of three-dimensional space where the values of the biomagnetic field are reconstructed using the algorithm described. The current dipole of the stomach is located in the space below the grid.

After completing the first recursive process described above—in which a first dipole location and its vector components had been found—the program was enhanced with the ability to add another dipole at a location different from that of the first dipole with the purpose of minimizing computational errors. For the implementation

of this task, the same approach was adopted as in the previous case described above. For the purpose of consistently testing the results of our algorithm, two different reconstruction assumptions were used in order to find current dipole locations as well as to calculate the values of the magnetic field. In the first approach to the numerical reconstruction, a single dipole was fit to the experimental data using the technique of least squares approximation. In the second one, the data was assumed to contain a minimum of two dipoles: one positioned in the upper half of the grid and the second one in the lower half. The computational errors in the numerically reconstructed magnetic field were then calculated. The computational scan for the first dipole was thus limited to the upper half of the grid, corresponding to the region in which the stomach was located. This was done in order to study the stomach signal as well as the one associated with the intestine. The dipole corresponding to the latter was assumed to be positioned within the lower half of the grid, a region to which the search for the second dipole was also limited. For each of the separate dipole search areas, a recursive scan was performed in which a considerably refined grid of points was used in order to identify the dipole location.

The program was designed so that the best fitting dipole could be found based on a combinatorial projection of one sequence of possible gastric dipole locations (in the upper grid section) with another sequence of possible intestinal locations (in the lower grid). For example, since four subsectors had to be scanned at the same time in each of the upper and lower sections of the grid at any recursive step, the best fitting dipole positions for the entire grid were found based on searching the best combinations of upper dipole positions and lower dipole positions. This was performed by reconstructing the field resulting from any possible combination of upper dipole and lower dipole locations according to the appropriate least squares criterion for this type of fit:

$$\frac{\partial}{\partial Q_x} \left[ \sum_{j=1}^n \sum_{k=1}^m (\tilde{B}_z^{jk} - \hat{B}_z^{jk} - \bar{B}_z^{jk})^2 \right] = 0 \quad (11)$$

$$\frac{\partial}{\partial Q_y} \left[ \sum_{j=1}^n \sum_{k=1}^m (\tilde{B}_z^{jk} - \hat{B}_z^{jk} - \bar{B}_z^{jk})^2 \right] = 0 \quad (12)$$

$$\frac{\partial}{\partial \bar{Q}_x} \left[ \sum_{j=1}^n \sum_{k=1}^m (\tilde{B}_z^{jk} - \hat{B}_z^{jk} - \bar{B}_z^{jk})^2 \right] = 0 \quad (13)$$

$$\frac{\partial}{\partial \bar{Q}_y} \left[ \sum_{j=1}^n \sum_{k=1}^m (\tilde{B}_z^{jk} - \hat{B}_z^{jk} - \bar{B}_z^{jk})^2 \right] = 0 \quad (14)$$

where  $\bar{B}$  stands for the magnetic field produced as a result of the presence of the second current dipole and  $\bar{Q}_x$  and  $\bar{Q}_y$  are its x and y vector components. In this second case, the corresponding function whose value was minimized becomes

$$(\chi^2)_i = \sum_{j=1}^n \sum_{k=1}^m \frac{(\tilde{B}_z^{jk} - \hat{B}_z^{jk} - \bar{B}_z^{jk})^2}{(\delta_z^{jk})^2} \quad (15)$$

showing that the value to be minimized is the difference between the experimental value of B as recorded by the magnetometer and the sum of the magnetic fields vector components resulting from the presence of the two dipoles. A set of SQUID channels was then chosen for which the experimental and computed values of  $B_z$  were plotted. In this manner, the value of the magnetic field obtained using the inverse solution was compared to the original, experimental value. For the entire data set of experimental magnetic field values, an average computational error level of 1.36% was obtained for the entire grid used in the simulation, corresponding to a B value of 2.0 femto-Amperes-meter.

All program modules were implemented in MathWorks™ MATLAB® version 6.1. The complete program was run on the COMPAQ Presario 7AP140 (7000 Series). The microcomputer that was used possessed the 800 MHz Athlon™ AMD processor with 128 MB of RAM as well as the 16 MB NVIDIA TNT2™ Graphics card. For a computational model in which the presence of only one gastric dipole was assumed, the time needed for a complete program run in which ten randomly-chosen time frames were processed was 10.32 minutes.

## 5. Visualization Techniques

The biomagnetic field visualization described here was accomplished using a computer-generated simulation written using the MATLAB programming language in which the binary data recorded by the SQUID magnetometer is processed directly. Because of the multiple aims of the scientific research presented, several important methods of visualization were used in order to ease the study of gastric biomagnetic behavior. In order to offer an accurate three-dimensional view of the biomagnetic field under analysis, the approach taken was identical to the one presented in the previous section: a three-dimensional array was created whose limits in the x and y plane were determined by the maximum and minimum positions of the SQUID input points, where the z coordinate of the measurement plane was taken to be equal to zero. The first important method of visualization that was used consisted of generating two-dimensional maps in which the vector components of the magnetic field  $\mathbf{B}$  were depicted. An example of this is presented in Figure 3. For each of the images shown, magnetic field values were calculated based on the current dipole position and orientation identified by the least-squares algorithm. Magnetic field values were then visualized based on a color map in which the highest biomagnetic field vector components values were depicted in dark red. The vector values with the lowest values are depicted in dark blue, while intermediate values are shown through the use of corresponding colors in the spectrum. This not only allows field positions to be easily identified, but also

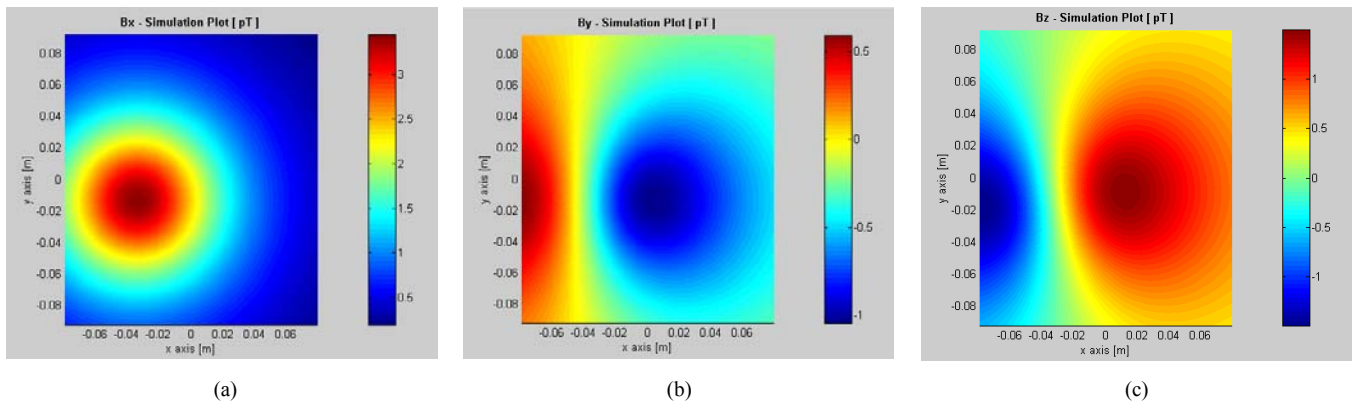


Figure 3. Maps of the vector components of the magnetic field  $\mathbf{B}$  i.e.,  $B_x$  (a),  $B_y$  (b), and  $B_z$  (c). Magnetic field units are pT (pico-Tesla). The current dipole had vector components  $(0.0167, -0.1642, -0.0894) \mu\text{A}\cdot\text{m}$  and its position was found to be  $x = -0.0342$  m,  $y = -0.0132$  m, and  $z = -0.0651$  m. All three maps were generated for the plane with equation  $z = 0$  m, implying that all  $\mathbf{B}$  were computed for a plane 6.51 cm above the dipole. In order to offer a color-based visualization of field magnitudes, legends are provided to the right of each plot. (a). Vector component values are highest directly above the dipole and decrease toward the outer edges of the grid as the distance from the dipole location increases, according to the Biot-Savart Law. (b). Since the  $\mathbf{i}$  and  $\mathbf{k}$  components of the magnetic field are negative, the orientation of the dipole confirms that the values of  $B_y$  are higher on the left side of the figure. (c). The orientation of the current dipole is emphasized more clearly by observing the orientation of the minima and maxima of  $B_z$ . The dipole is oriented along the separating line toward the lower side of the figure and inside the page since the  $z$  component of the magnetic field is negative.

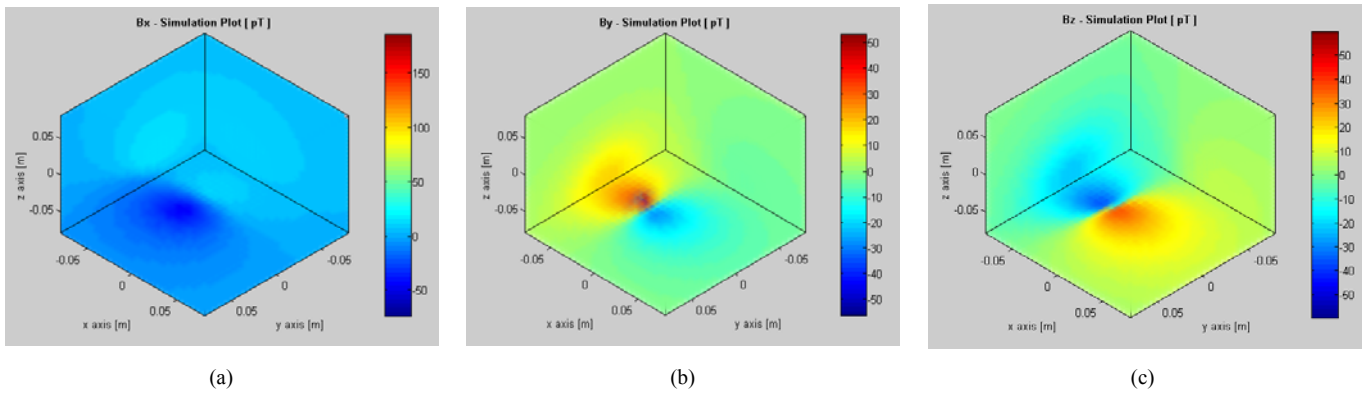


Figure 4. Three-dimensional visualization of biomagnetic field components originating in the abdomen. Dipole locations and orientations are identical to those in Figure 3. The units used for the magnetic field are pT. The vector components  $B_x$ ,  $B_y$ , and  $B_z$  respectively are visualized for a tetrahedron where the abdomen is located below the plane  $z = 0$ , i.e. in the lower half of the volume. The magnetic field visualization is viewed from the left below, from an azimuthal point of  $-45^\circ$  and an elevation of  $-45^\circ$ .

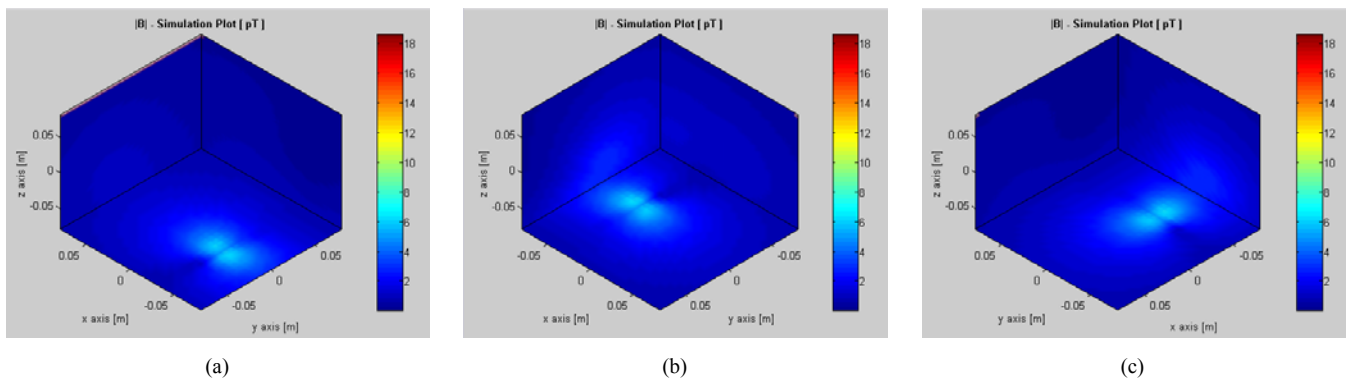


Figure 5. Visualization of the magnetic field magnitude  $|\mathbf{B}|$  in three-dimensional space for the dipole locations and orientations given in Figure 3. In (a), the magnetic field reconstruction volume is viewed from an azimuth of  $135^\circ$  and an elevation of  $-45^\circ$ . The dipole location is visible at the center of the brighter, higher-magnitude field. In (b), the reconstructed field is viewed from the left below (azimuth of  $-45^\circ$ , elevation of  $-45^\circ$ ), where an interesting region of dipole magnitude decrease is visible on the vertical limit of the volume. In (c), the perspective point is located at the back right below (azimuth =  $-135^\circ$ , elevation =  $-45^\circ$ ).

reveals the configuration and magnitude of the field, which is not otherwise apparent using ordinary visualization procedures. Magnetic field values were then

generated in three-dimensional space within a tetrahedron, as depicted schematically in Figure 2 and exemplified with realistic experimental magnetic field

values in Figure 4. Due to the fact that the current dipole is located in the stomach for each of these situations depicted, the values of the field are stronger in the lower portion of the volume in which these values of  $\mathbf{B}$  were computed. In addition to generating visualizations of  $\mathbf{B}$  vector components separately, images were also created for the magnetic field magnitude in the space described. The result of such a computation is shown in Figure 5. Concerning the actual three-dimensional reconstruction of the field, a shell model of field magnitude intensity was used in order to produce an accurate view of how the dipole is configured. The proportionality between the decrease in the magnitude of the magnetic field and the distance to the current dipole was made visible by assigning a “magnitude shell” to each magnitude range of levels. As the distance from the observation point to the current dipole increases, the magnitude of the magnetic field decreases and thus the magnetic field values are represented in 3D space through the use of the corresponding magnitude shell, which is shown in a different color, according to the color map. In each of these cases, the reconstruction tetrahedron was viewed from the left below (azimuth of  $-45^\circ$  and elevation of  $-45^\circ$ ) as well as from directly below (azimuth of  $0^\circ$ , elevation of  $-90^\circ$ ). In the first choice of viewpoint, the y axis increases to the left of the observer, the x axis increases to his/her front, and the z axis upwards. In the second case, the observer lies horizontally directly below the reconstruction volume. The y axis increases to his/her right, and the z axis upwards. In order to enhance the visual quality of the rendering, magnetic field values were logarithmically scaled according to the piecewise scaling function

$$B_n(B_o) = \begin{cases} -\ln(1 - B_o) & B_o \in (-\infty, 0) \\ \ln(B_o + 1) & B_o \in [0, +\infty) \end{cases} \quad (16)$$

where  $B_n$  represents the scaled value of the magnetic field component as a function of  $B_o$ , which stands for its original value. Applying the scaling function above allowed the lower magnetic field values to be more visible in the three-dimensional visualization, due to the fact that the color map was designed based on the extreme values of the biomagnetic field.

## 6. Interpretation and Applications

An important fact that stems from the visual nature of this reconstruction is that multiple dipoles can be easily detected and studied. The direction of the streamline vector plots gives an accurate image of the electromagnetic field configuration for the stomach region under investigation. An immediate practical result of this is that secondary dipoles can be identified in the experimental data sets. The behavior of current dipoles in the stomach interestingly opens the way to further investigations of the underlying theoretical model that best predicts stomach magnetic conditions for a variety of pathological cases. Another essential observation is that

the periodicity of bioelectric current propagation can be observed in a three-dimensional visualization environment. Numerous other directions of scientific inquiry were made obvious throughout the development of the research project presented above. It was determined that there is an acute need of depicting the biomagnetic field of the stomach in a highly realistic manner, which necessarily involves computations based on experimental initial-value data taking into account the existence of several dipoles in the stomach. Following the latest results in this field, the dipole should also be modeled as being located at a variable depth with respect to the measurement plane.

## 7. Summary and Conclusions

Magnetic field pattern-recognition algorithms are necessary for the straightforward identification of interesting points and for the automated computation of field values. Due to the unpredictable nature and great complexity of living-state physical systems, this appears to be an efficient manner of maintaining a high level of precision that would make the predicted magnetic field values agree with experiment to the highest degree. Studying the biomagnetic field of the stomach is of great importance in the process of early diagnosis and treatment of various diseases. The visual tool that has been developed offers not only a good way of predicting its values for positions outside the data-sampling region, but it is also an efficient manner of analyzing how various configurations correspond to the magnetic field patterns that are of interest for medical diagnosis.

## 8. Acknowledgements

Funding for this investigation was made available by the Veterans' Affairs Research Service, NIH Grant R01 DK 58697-01 and by the College of Natural and Applied Sciences at Lipscomb University.

## References

- [1]. S. Baillet, K. Jerbi, R. M. Leahy, J. C. Mosher, On MEG Forward Modelling Using Multipolar Expansions, *Physics in Medicine and Biology*, 47 (3), 2002, 523-555.
- [2]. J. Mosher, R. M. Leahy, Source Localization Using Recursively Applied and Projected (RAP) MUSIC, *IEEE Transactions on Signal Processing*, 47 (2), 1999, 332.
- [3]. J. Sarvas, Basic Mathematical and Electromagnetic Concepts of the Biomagnetic Inverse Problem, *Physics in Medicine and Biology* 32 (1), 1987, 11-22.
- [4]. J. C. Mosher, R. M. Leahy, Recursive MUSIC: A Framework for EEG and MEG Source Localization, *IEEE Transactions on Biomedical Engineering* 45 (11), 1998, 1342-1355.
- [5]. J. C. Mosher, R. M. Leahy, EEG and MEG: Forward Solutions for Inverse Methods, *IEEE Transactions on Biomedical Engineering* 46 (11), 1999, 245.